Simplified Analysis of Kinescope Electron Guns

D. A. de Wolf*
RCA Laboratories, Princeton, NJ 08540

Abstract—The numerical integration of trajectory equations to simulate electron beams in kinescope electron guns is complicated because (a) the interior electrostatic fields cannot be computed analytically and (b) space-charge forces couple the trajectory equations to the Poisson equation nonlinearly. Solution by digital computer requires iteration of trajectories and storage of large arrays of potentials, fields, and current densities. Even exploratory analysis can be costly. A simplified analysis is presented here that permits speedy, low-cost evaluation of axially symmetric electron guns, albeit at a loss of high accuracy. The analysis utilizes approximations to the lens fields and to the Coulomb forces in various gun regions. The approximations are especially good in the drift and main-lens regions.

1. Introduction

The design of kinescope electron guns has been greatly enhanced by the ability to simulate electron trajectories numerically with digital computers.[1,2] To do so, one needs to solve the usual[3] second-order differential equations of the trajectory coordinates as functions of time or of the axial coordinate. The differential equations involve the potentials and fields of the regions through which the electrons pass. In all but the most elementary situations, even with known fields and potentials everywhere, it is necessary to integrate the trajectory equations numerically. The techniques are standard[4,5] and pose no particular problem.

However, two factors greatly complicate the numerical integration

*Presently at Virginia Polytechnic Institute and State University, Dept. of Electrical Engineering, Blacksburg, VA 24061.

of trajectory equations. First, if space charge (the mutual Coulomb forces between electrons) is ignored, then the potential is obtained from the Laplace equation with appropriate boundary conditions.[3,6] Numerical methods are nearly always needed. Relaxation methods[7,8] require calculation of a large two- or three-dimensional array of fields, and integral-equation methods[5] either require this also or necessitate repeated evaluation of potential and fields by a time-consuming numerical integration at each trajectory point.

In the second place, space charge renders the differential equations, together with the needed Poisson equation, nonlinear because the fields depend upon (to be calculated) trajectory coordinates. The numerical work is greatly increased by the necessity of an iteration procedure[8,9] through enough cycles so that the fields calculated from the $(n-1)$st trajectory coordinates do not bring about appreciable modifications in the nth trajectory coordinates.

In practice, kinescope electron guns are manufactured from more-or-less standard parts, and one can separate a gun into three regions: a beamforming region (BFR) in which several round-aperture lenses extract and concentrate a beam of electrons emitted from a cathode; a main-lens region (MLR) in which the diverging beam is focussed towards a screen location; and a drift region (DR) in which the redirected electrons move only under space-charge and deflection forces to a relatively distant screen.

Alig[10] has recently reviewed these and related matters. A characteristic sketch is shown in Fig. 1 to clarify the separation. The main lens usually consists of several metallic cylinders of equal radius placed coaxially in tandem to produce a compound-cylinder lens with small gaps between the components.

For much design work with kinescope guns and certainly for the initial determination of operational parameters such as focus voltage, drive-voltage versus current characteristics, etc., it seems unnecessary to demand high accuracy of the trajectory simulation. The purpose of this paper is to present analytical approximations to potentials and fields everywhere that vastly reduce the numerical work to merely the one-time numerical integration of a set of second-order ordinary differential equations with known coefficients under appropriate initial conditions.

A full numerical program, ELOP,[8] has been utilized to provide a standard calculation to which the approximations of this work can be compared. Certain assumptions regarding the fitting of a beam current density to sample trajectory coordinates have been made in ELOP; similar ones have been utilized in this work to make a comparison feasible. The approach is four-fold:

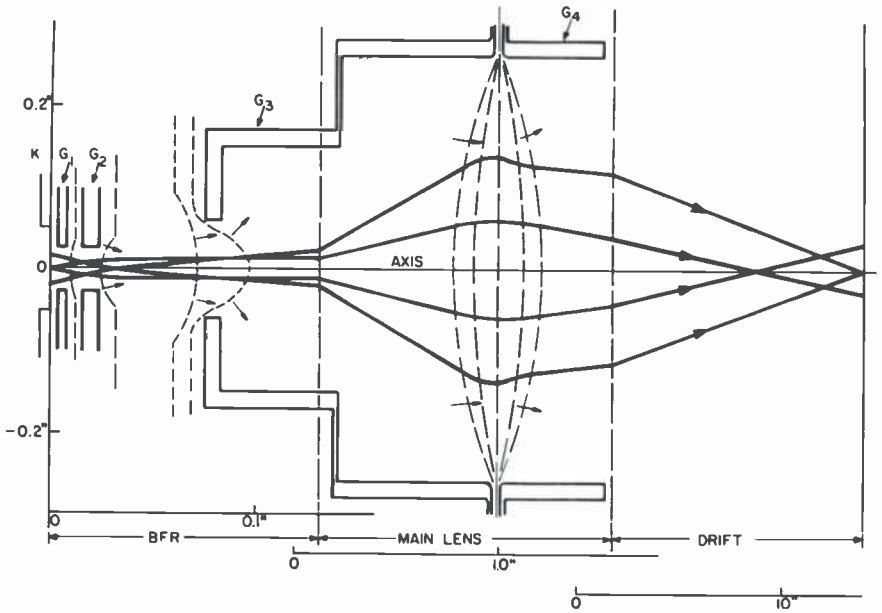

Fig. 1—Sketch of a kinescope emphasizing the electron optics aspects (from Alig, Ref. [10]). Note that G3 and G4 have effectively the same radius with respect to the lens formed by both electrodes. The various regions are drawn to different scales. Some equipotential lines (dashed) and some key trajectories (heavy lines) are depicted.

(1) Replacement of the space-charge fields by an equivalent transverse field. Neglect of longitudinal fields is serious only close to the cathode in the BFR [see point (4) below], and it eliminates the need for iteration.

(2) Approximation of potentials and fields inside the main lens by a two-term analytical approximation based on an extension of Bertram's approximation[11] for axially symmetric cylinders of equal radius.

(3) Approximation of potential and fields inside the BFR by an extension of an analytical procedure due to Regenstreif[12] for compound coaxial aperture lenses.

(4) An analytical determination of the emitted current profile and the concomitant analytical calculation of electron trajectories with Child's law under the space-charge limited conditions close to the cathode.

Because the complexity of these approximations is greatest nearest the cathode, and least in the DR, we shall examine them in reverse order of the actual cathode-to-screen calculation. Thus, we start with the DR, where there are only space-charge and deflection fields; we

then discuss the MLR, where space-charge fields are small but where there are lens forces; and we end with BFR where both forces are strong. An estimate of current density also is obtained from the BFR parameters.

2. The Transverse Space-Charge Approximation in the Drift Region.

The electron beam enters the drift region from the MLR and may undergo deflection forces to focus upon a spot that is not at the center of the screen. Whether or not the beam is deflected, however, the only electrostatic forces in the DR are due to space charge. Each electron can be considered to be in a central-force field due to the collective effect of all other electrons.[13] This field is

$$E(R) = \frac{-e}{4\pi\epsilon_0} \int d^3R_1 n(\mathbf{R}_1) \frac{(\mathbf{R} - \mathbf{R}_1)}{|\mathbf{R} - \mathbf{R}_1|^3}, \qquad [1]$$

where $n(\mathbf{R}_1)$ is the number density of electrons at $\mathbf{R}_1$, e is the electron charge, and ϵ_0 is the vacuum dielectric permittivity. Consider a reference trajectory in the beam, e.g., a central trajectory. It has a longitudinal coordinate ζ_1. All other electrons can then be characterized by the locally orthogonal coordinate system $\mathbf{R}_1 = (\rho_1, \zeta_1)$ where ρ_1 has two mutually orthogonal components that need not be specified further.

Typical electron beams in the drift region have a density $n(\rho_1, \zeta_1)$ that varies slowly with ζ_1. Characteristically, there will not be much change in $n(\rho, \zeta_1)$ for a length of several radii of the beam in the longitudinal direction. It is not difficult to perform the $d\zeta_1$ integration in Eq. [1] under the approximation that $n(\mathbf{R}_1)$ does not depend upon ζ_1, and that there is no curvature locally over several beam radii. We then obtain

$$E(\rho, \zeta) = -\frac{e}{2\pi\epsilon_0} \int d^2\rho_1 n(\rho_1, \zeta) \frac{(\rho - \rho_1)}{|\rho - \rho_1|^2}. \qquad [2]$$

The same result can be obtained by applying Gauss's law to a thin pillbox perpendicular to the reference trajectory. The two surface forces on the top and bottom of the pillbox almost cancel each other, and in the approximation they are consequently neglected. The remaining terms can be shown to lead to Eq. [2], which obviously results from ignoring the longitudinal space-charge forces. The result, Eq. [2] is much more advantageous in use than Eq. [1] not only because it represents a two-dimensional integral (instead of a three-dimensional

one) but especially because $E(\mathbf{R})$ depends only on values of $n(\mathbf{R}_1)$ with $\zeta_1 \leq \zeta$. This crucial fact eliminates the nonlinearity, hence also the need for an iterative numerical procedure. The remaining numerical procedure then consists, in the absence of deflection, of solving the equations of motion which we give in nonrelativistic form in the standard cylindrical coordinate system,[14]

$$\mathbf{r}'' = \frac{(1 + \mathbf{r}'^2)}{2\Phi(\mathbf{r}, z)} [\mathbf{E}_r(\mathbf{r}, z) - \mathbf{r}' E_z(\mathbf{r}, z)]. \qquad [3]$$

Here, $\mathbf{E}_r$ and E_z are the three mutually perpendicular components of the field given in Eq. [2] [and $\mathbf{r}$ is a vectorial notation for the x and y components].

It is obviously necessary to discretize the beam into a number of beamlets. Then, Eq. [2] becomes

$$E(\mathbf{R}) = \frac{e}{2\pi\epsilon_0} \sum_m \int_{S_m} d^2\rho_1 n(\rho_1, \zeta) \frac{(\rho - \rho_1)}{|\rho - \rho|^2}, \qquad [4]$$

where S_m is the cross-sectional area of the mth beamlet. The beamlet is represented by one trajectory $\mathbf{r}_m(z)$ which is governed by Eq. [3]. The remaining problem is to choose the areas S_m conveniently in shape and size. Actually, a much more important problem arises here: that of beam representation. Quite in general, the number density $n(\rho_1, \zeta)$ is itself a two-dimensional integral over velocities (or momenta p_1) in the z plane characterized by ζ (the variation of ζ across the beam in a z plane is ignored)

$$n(\rho_1, \zeta) = \int d^2p_1 f(\rho_1, \mathbf{p}_1; \zeta). \qquad [5]$$

Hence Eq. [2] is actually a four-dimensional integral over a phase-space density f, and discretization should occur in all four dimensions. In this work we assume that the discretization in momentum has already been chosen prior to the DR; this is discussed later. It is by no means a trivial point because beam reconstruction at the screen is very difficult for deflected beams, even when all chosen trajectories are simulated accurately. However, we will restrict ourselves largely to rotationally symmetric beams (i.e., without deflection) in which case the momentum discretization is less of a problem.

A square mesh with spacing h is convenient for reducing Eq. [4] under the assumption that $n(\rho, \zeta)$ of the meshblock characterized by its center at $\rho_{mn} = (x_m, y_n)$ is constant. This approximation determines the magnitude of h for desired accuracy. The resulting integral in Eq.

[4] over squares can be performed and it gives

$$\mathbf{E}(\mathbf{R}) = -\frac{e}{2\pi\epsilon_0}\sum_{m,n} n(\rho_{mn}, \zeta)\mathbf{G}^{(mn)}, \quad \text{with}$$

$$G_x^{(mn)} = \frac{1}{2}t_f \ln[(t_f^2 + s_f^2)/(t_f^2 + s_i^2)]$$

$$-\frac{1}{2}t_i \ln[(t_i^2 + s_f^2)/(t_i^2 + s_i^2)] \qquad [6a]$$

$$+ s_f[A(t_f/s_f) - A(t_i/s_f)]$$

$$- s_i[A(t_f/s_i) - A(t_i/s_i)],$$

where $A(t/s)$ is an abbreviation for the arctangent of t/s, and the arguments of the functions in Eq. [6a] are defined by

$$\begin{aligned} s_f &= (x - x_m) + h/2, \qquad t_f = (y - y_n) + h/2 \\ s_i &= (x - x_m) - h/2, \qquad t_i = (y - y_n) - h/2 \end{aligned} \qquad [6b]$$

A similar expression holds for the y component of $\mathbf{G}^{(mn)}$. These expressions can be greatly simplified if one is willing to allow for some inaccuracy in the vicinity of the edges of the square

$$\mathbf{G}^{(mn)} \sim \frac{(\rho - \rho_{mn})}{|\rho - \rho_{mn}|^2 + h^2/\pi}. \qquad [7]$$

The error can be shown to become negligible as $h \to 0$. In practice, even for a relatively coarse mesh, the error can be kept small because most of the contribution to $E(R)$ in Eq. [4] comes from nonneighboring meshblocks. Admittedly, there may be z planes in which $n(\rho_{mn}, \zeta)$ is very granular in distribution, but even then the forces are most important where Eq. [7] is a good approximation to Eq. [6].

In the case of a rotationally symmetric beam, we may choose $\zeta = z$, and $\rho = r$, and Eq. [2] can then be reduced to

$$E(R) = \frac{e}{\epsilon_0 r_0}\int_0^r dr_1 r_1 n(r_1, z), \qquad [8]$$

where the transverse space-charge field E is now directed radially outwards and is denoted as a scalar in Eq. [8]. A discretization of Eq. [8] is trivial, as the singularity problem is removed by the azimuthal integration of Eq. [2] leading to Eq. [8]. However, some discussion follows because of the beam representation problem. The quantity $-en(r_1, z)$ is the charge density which is equal to $j(r_1, z)/v(z)$ in terms of the current density and velocity at z (we ignore the very minor variation in velocity with r_1). Thus Eq. [8] becomes (with $v \propto \Phi^{1/2}$)

$$E(R) = \frac{\beta}{r\Phi^{1/2}}\int_{r_1<r} d^2 r_1 j(r_1), \qquad \beta \equiv \frac{(m/2e)^{1/2}}{2\pi\epsilon_0}, \qquad [9]$$

where we have chosen to write the integral in a more general fashion even though $j(r_1)$ is rotationally symmetric. Here, Φ is the (constant) potential in the drift region; it is high enough to ignore the small contribution of the initial electron kinetic energy. The fact that $d^2r_1 j(r_1)$ of an annulus of current arises from a cathode annulus $d^2r_c j(r_c)$ can be used to construct the former from an initial cathode discretization. We assume that,[8, 15]

$$j_c(r_1) = \frac{1}{\pi\sigma^2} \int d^2r_2 j_p(r_2) e^{-(r_1 - r_2)^2/\sigma^2}, \qquad [10]$$

where $j_p(r_2)\, d^2r_2$ is the total current emitted in an annulus d^2r_2.

ELOP assumes that the integral (Eq. [10]) can be reconstructed from three electrons that enable us to determine the center and $1/e$ width of the Gaussian by fitting moments. Here, Eq. [9] is discretized into $3N$ pieces (with $3N$ trajectories) associated with Eq. [3]. The result for Eq. [9] is

$$E(R) = \frac{2\pi\beta}{r\Phi^{1/2}} \sum_{n=0}^{N-1} \sum_{i=1}^{3} a_i n h_c^2 j_c(n h_c) \theta(r_{ni} - r), \qquad [11]$$

where θ is the Heaviside stepfunction that is zero for negative and unity for positive argument. Here, h_c is the discretization interval, and

$$a_1 = (1 + 2e^{-1})^{-1}, \qquad a_2 = a_3 = e^{-1} a_1, \qquad [12]$$

represent the discretization of the Gaussian thermal distribution into three electrons, one at the peak value and two at $1/e$ values, all in one meridional plane with the axis.

It is useful to gun designers to know the ultimate slit current $j_s(r)$ defined as

$$j_s(x) \equiv \int_{-\infty}^{\infty} dy\, j(x, y) = 2 \int_x^{\infty} dr \frac{r j(r)}{(r^2 - x^2)^{1/2}}. \qquad [13]$$

The slit current $j_s(x)$ can be calculated from Eqs. [13], [10], and the approximations underlying Eq. [11] by means of an algorithm developed by Campbell.[8] Only $3N$ electrons need be traced from the cathode on, where N is an integer of the order of 10, to obtain beam representations accurate to well within 5% of ELOP-calculated kinescope beams. Figs. 2 to 4 show comparisons of the above approximations to results obtained from a full-scale computer simulation with the RCA electron-optics program ELOP.[8]

Because space-charge forces are proportional to current density and to length squared, agreement is best in Fig. 2, which simulates a 1.5-mA beam in the DR of a relatively short kinescope. The effect of space

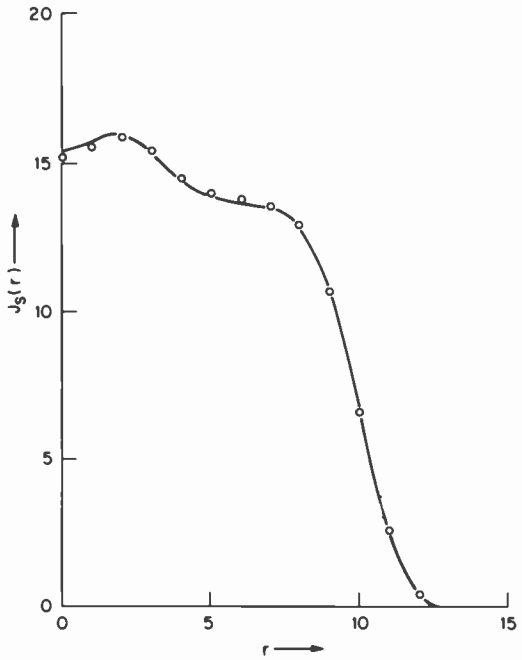

Fig. 2—Slit current $J_s(r)$ in arbitrary units at the screen versus r for the full numerical simulation (curve) and for approximation of the space charge forces based on Eq. [11] (circles). The drift parameters are L = 7.06 inches, V = 30 kV, and I = 1.5 mA.

charge is clearly not negligible at 3.5 mA, as can be seen in Fig. 3, so that it must be incorporated in simulations of typical high-intensity TV screen spots. The shape of the beam of Fig. 3 was varied to produce the quite differently shaped spots in Fig. 4. In all cases, agreement is close to or within the accuracy of the ELOP program.

Beam representation of asymmetric beams is much more difficult because the integral in Eq. [10] is then essentially two-dimensional so that azimuthal smoothing cannot be taken advantage of. However, several symmetric beams were subjected to the more general space-charge field approximations Eqs. [6, 7], and the resulting symmetric spot provided a radial distribution of final screen coordinates $r_m (1 \leq m \leq 3N)$ that could be processed with the azimuthal smoothing as above. In Figs. 5 and 6, two cases are compared with results of the ELOP program. The beam in Fig. 5 is the same as that in Fig. 3; agreement with the numerical computer simulation is perhaps fortuitously good. The beam simulation in Fig. 6 illustrates an interesting aspect of the asymmetric approximations; the mesh choice $N_{sc} = 11$ gives a poorer result than $N_{sc} = 9$. The reason is that the number of space-charge meshblocks, N_{sc}^2, must not be so large that the smoothed number density is granular (i.e., so that there are only a few, or less, electrons

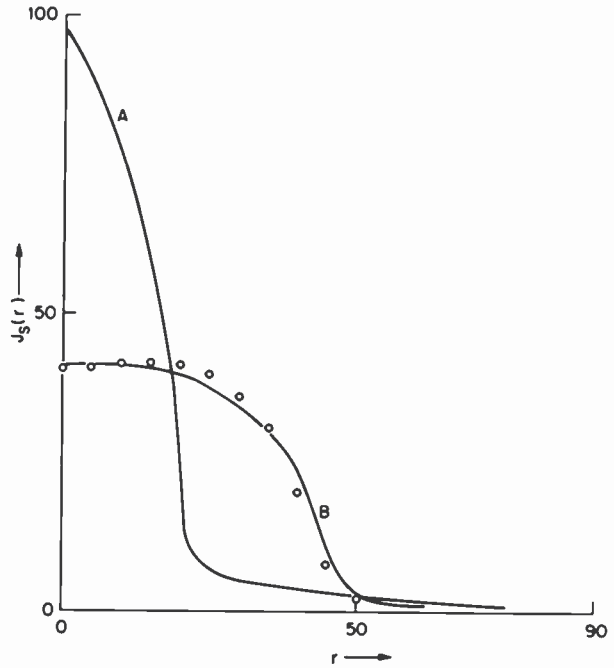

Fig. 3—Slit currents $J_s(r)$ versus r for a drift region with L = 13.5 inches, Φ = 30 kV, and I = 3.5 mA, without space charge (A) and with space charge (B). The circles show the transverse space charge approximation based upon Eq. [11].

per meshblock). The granularity introduces errors in the space-charge forces (Eq., [7]) where the denominators can become too small. On the other hand a very low value of N_{sc} will smooth out the space-charge forces too much. Apparently N_{sc} = 9 is close to an optimal choice as shown in Fig. 6.

3. Field Approximations in the Main Lens Region

The electron beam, having passed a crossover region in the BFR, enters the first cylindrical field-free region of the MLR and is refocussed towards the center of the screen by one or several more cylindrical-lens parts. It then exits into the DR in a field-free region at the so-called ultor voltage[10] of the rest of the kinescope vacuum tube. It is customary to use two or more coaxial cylindrical metallic tubes, all of the same radial extent interspaced with small gaps, as main lens. Each cylinder is given its own voltage, which is maintained during operation of the tube.

It is well-known[6, 16] that the interior of a cylinder of radius R with a boundary potential profile $\Phi(R, z) = V(z)$ (where z is the axial

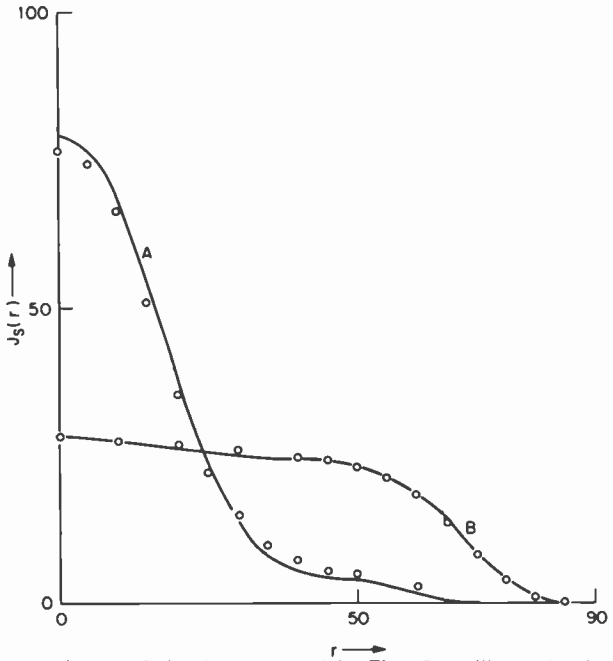

Fig. 4—Two variants of the beam used in Fig. 6 to illustrate the effect of varying electron trajectories in a drift region. An overfocussed beam (A) and underfocussed beam (B) give slit currents evaluated by computer (curves) and with Eq. [11] (circles).

direction) is governed by a potential

$$\Phi(r, z) = \frac{1}{2}\int_{-\infty}^{\infty} dz_1 V(z_1) g(r, z - z_1),$$

$$g(r, \zeta) \equiv \frac{2}{\pi}\int_0^{\infty} dk \frac{J_0(kr)}{J_0(kR)} \cos(k\zeta), \qquad [14]$$

with modified Bessel functions $J_0(kr)$ and $J_0(kR)$ in the Green's function $g(r, \zeta)$. Under the reasonable (and tested) assumption that $V(z)$ is constant on a metallic cylinder and linear in the gaps, Eq. [14] can be reduced to

$$\Phi(r, z) = \frac{1}{2}(V_0 + V_N) + \frac{1}{2}\sum_{n=1}^{N} \frac{V_n - V_{n-1}}{d_n} \int_{z_n}^{z_n + d_n} dz' G(r, z - z')$$

$$G(r, \zeta) \equiv \frac{2}{\pi}\int_0^{\infty} dk \frac{J_0(kr)}{k J_0(kR)} \sin(k\zeta). \qquad [15]$$

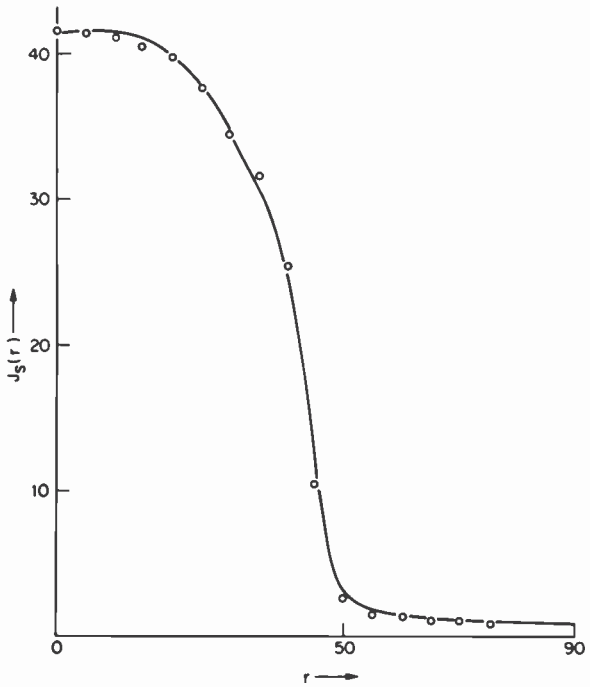

Fig. 5—Slit current $J_s(r)$ versus r for the same situation as in Fig. 3. The transverse space-charge approximation (circles) is evaluated as if the beam were asymmetric with Eq. [7].

The geometry is depicted in Fig. 7. Although the dz' integration can be performed in closed form, it is preferable to write it as above at this stage. The interior potentials (and fields) are thus given as an integral over an oscillatory integrand that must be evaluated numerically. The slow oscillatory asymptotic decrease of the integrand requires many steps in the numerical evaluation. Apparently the evaluation of Eq. [15] offers no clear numerical advantage over the numerical solutions[5] of Laplace's equation in a cylindrical region.

However, Bertram[11] found as early as 1940 that the function $G(0, \zeta)$ is simulated to within 6% errors for $|\zeta| \leq 1.5R$ by the function

$$G_B(0, \zeta) = \tanh(1.318\, \zeta R). \qquad [16]$$

This approximation of the axial Green's function can be improved[17] to give better than 2% accuracy with a two-term version of Eq. [16]

$$G_A(0, \zeta) = A_1 \tanh(w_1 \zeta/R) + A_2 \tanh(w_2 \zeta/R), \qquad [17]$$

with $A_1 = 0.800987$, $A_2 = 1 - A_1$, $w_1 = 1.20241$, $w_2 = 1.82456$ to six

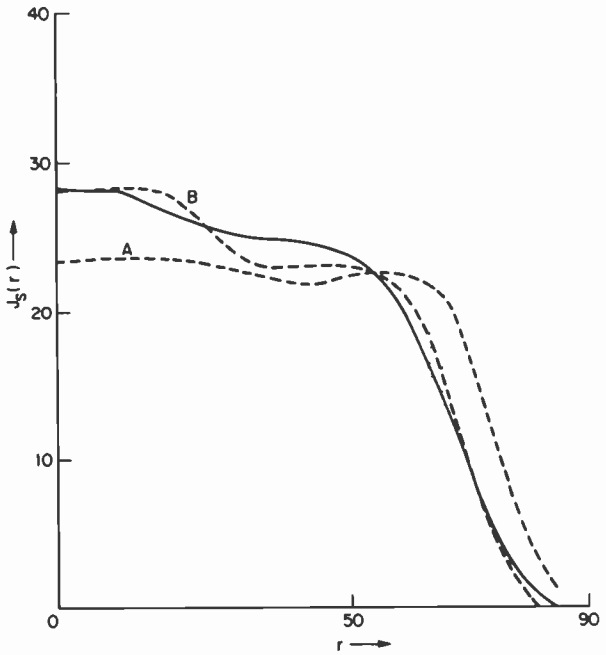

Fig. 6—Slit current $J_s(r)$ versus r for a drift region with L = 13.5 inches, Φ = 20 kV, and I = 3.5 mA (full curve) compared to two calculations based on Eq. [7]: (A) with N_{sc} = 11 and (B) with N_{sc} = 9.

significant figures. The result for $\Phi(0, \zeta)$ is,

$$\Phi(0, z) = \frac{1}{2}(V_0 + V_N) + \frac{R}{2}\sum_{n=1}^{N}\frac{V_n - V_{n-1}}{d_n} \sum_{i=1}^{2} A_i \ln\left\{\frac{\cosh[w_i(z - z_n)/R]}{\cosh[w_i(z - z_n - d_n)/R]}\right\}. \quad [18]$$

The off-axis contributions can be obtained from the symbolical form,

$$\Phi(r, z) = J_0(r\partial/\partial z)\Phi(0, z), \quad [19]$$

where the Bessel function $J_0(r\partial/\partial z)$ is expanded into its Taylor series as if $\partial/\partial z$ were a coefficient of r. The functions in Eq. [18] are analytically differentiable, so that off-axis potentials and fields are easily generated from Eqs. [18] and [19]. The four coefficients in Eq. [17] are obtained by fitting the derivative $G_A'(0, \zeta)$ to $g(0, \zeta)$ at $\zeta = 0$, and at $\zeta = \infty$ using the asymptotic expansion of $g(0, \zeta)$.[18] Thus, an inexpensive simulation of electron beams in standard cylindrical ML lenses can be obtained from numerical integration of the trajectory equations Eq. [3] with additive electrostatic fields approximated by

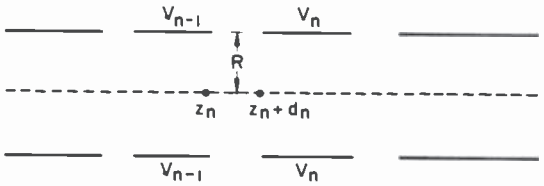

Fig. 7—Sketch of the geometry of a compound axially symmetric cylinder lens with coaxial, equi-radius components.

Eq. [11] for the space-charge forces and by Eq. [18] and [19] for the Laplace forces due to the lens.

A simulation due to lens effects alone is given in Table 1. Here, two cylinders with radius $R = 100$ units (1 inch is 1000 units*) have been chosen. The gap between them is $0.5R$ wide and it lies at $5R$ from the input plane. The output trajectory coordinates r and r' lie at $8.5R$ from the input plane. The input coordinates are not given, but they arise from seven triplets leaving the cathode in one plane containing the axis. Each triplet is emitted at $r_c = m$ units above the axis ($0 \leq m \leq 7$) with $r_c' = -1$ (−sign), 0, or +1 (+sign). Fig. 8 illustrates the trajectories of the $r_c' = 0$ electrons in this region.

The effect of space charge can be shown to be small in this region.

Table 1—Comparison of r,r' in an MLR

r_c	ELOP		2-Term Bertram	
	r	$r' \times 10^3$	r	$r' \times 10^3$
+0	−2.65	0.30	−2.68	0.21
−1	6.06	0.50	6.15	0.71
1	0.47	0.17	0.48	0.19
+1	1.69	1.08	1.72	1.14
−2	8.93	1.19	9.06	1.49
2	5.62	1.20	5.71	1.40
+2	6.45	1.20	6.56	2.22
−3	11.93	1.67	12.12	2.11
3	10.20	1.98	10.35	2.34
+3	11.32	2.73	11.49	3.12
−4	14.67	2.03	14.88	2.53
4	15.27	2.60	15.49	3.12
+4	16.56	3.18	16.81	3.76
−5	19.16	2.21	19.43	2.86
5	20.00	2.78	20.28	3.42
+5	22.54	3.07	22.88	3.89
−6	23.00	1.78	23.33	2.56
6	24.90	2.20	25.25	3.04
+6	28.64	2.00	29.02	2.91
−7	25.86	0.16	26.23	1.09
7	29.23	0.36	29.63	1.35

* One inch is 1000 mils in engineering terminology. I prefer to use the word "unit" because absolute lengths need not be specified in general.

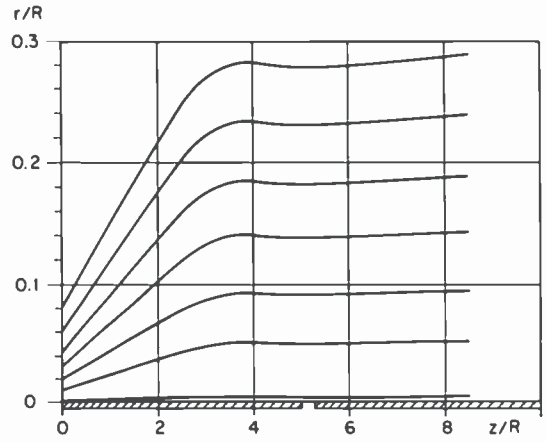

Fig. 8—The trajectories (which lie in one plane through the axis) of seven principal electrons traversing a two-cylinder lens with gap length $0.5R$ and voltage ratio 0.24.

It was excluded from the above example to separate out the effect of the lens approximation. The accuracy in Table 1 is not unreasonable. An error in r' of 0.0004 yields only a 5.5 unit error in r at 13.5 inch (13,500 units) beyond the exit plane, which is acceptable in kinescope spot analysis, at least in an initial determination of parameters.

4. Field Approximations in the Beamforming Region

The analysis of electron trajectories is most difficult in the BFR. While it is true that a (thermionic) cathode emits electrons under the influence of a shaped electric field created by appropriate voltages on the BFR electrodes labeled $G1$ and $G2$ (see Fig. 1), this emission is initially space-charge limited.[19,20] That is to say that the space-charge forces are dominant in the region very close to the cathode (of one to two length units extent, typically), and, moreover, they are largely longitudinal, not transverse. Thus, the electrostatic fields differ sharply from those due to the lens elements alone in this "diode region", and the transverse-space-charge approximation does not apply.

Furthermore, even though a rapid transition takes place beyond the diode region to one in which Laplace forces dominate, the current modulation properties of the $G1$ and $G2$ electrodes force the principal electrons (those with no transverse velocity at the cathode) to cross over the axis somewhere between $G1$ and $G2$ so that relatively large space-charge forces may again occur in a restricted "crossover region."

The analysis by which electron trajectories through the diode region are calculated is postponed until the next section. The input for the

work in this section is a diode plane several units beyond the cathode with values of r and $r' = dr/dz$ of the electron coordinates.

The analytical model for each aperture electrode in the BFR is a pair of infinitesimally thin perfectly conducting plates at voltage V with circular apertures of radius R coaxial with the gun axis. The analytical expression for the potential that arises from one of these in isolation with asymptotic fields E_L (at $z = -\infty$) and E_R (at $z = \infty$) is well known:[21]

$$\Phi(r, z) = V - \frac{1}{2}(E_L + E_R)z + \frac{1}{\pi}(E_L - E_R)|z|\left[A(u) + \frac{1}{u}\right], \quad [20]$$

where $A(u) \equiv \arctan(u)$, and

$$u^2 = \frac{1}{2R^2}\{(r^2 + z^2 - R^2) + [(r^2 + z^2 - R^2)^2 + 4R^2z^2]^{1/2}\}. \quad [21]$$

Regenstreif[22] found that $\Phi(0, z)$ for a coaxial set of three such aperture lenses could be given by a linear superposition of the $r = 0$ versions of Eqs. [20] and [21]. The idea of superposition has been generalized to more than three apertures and to off-axis potentials. Specifically, the BFR is modeled as shown in Fig. 9. Each of the two grids, $G1$ and $G2$, is modeled by a pair of aperture lenses at the same

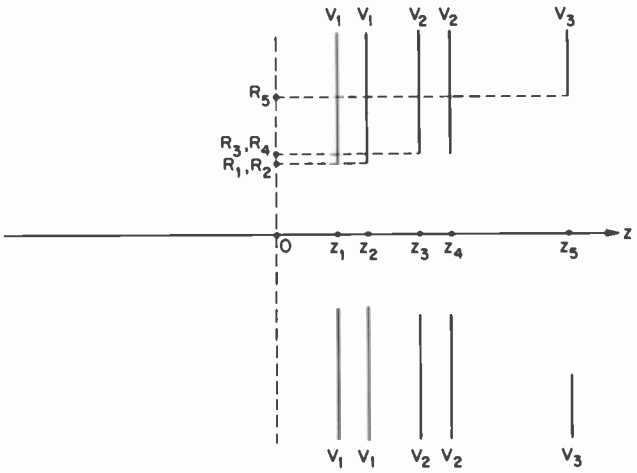

Fig. 9—Sketch of the BFR model by means of circular apertures. Only half of the total number of apertures are shown.

voltage. The entrance to the $G3$ grid requires only one further aperture lens at voltage V_3. To ensure a zero cathode voltage, the $z = 0$ plane is the result of an antisymmetric distribution of 10 aperture lenses in total; each of the 5 sketched ones in Fig. 9 has an antisymmetric counterpart at $z = -z_m$ with $V = -V_m (m = 1, \cdots, 5)$. The electrostatic potential is then approximated by

$$\Phi(r, z) = \sum_{m=1}^{5} \Phi_m(r, z)$$

$$\Phi_m(r, z) = \frac{1}{\pi} E_m \left\{ | z + z_m | \left[\frac{1}{u_m^+} + A(u_m^+) \right] \right.$$

$$\left. - | z - z_m | \left[\frac{1}{u_m^-} + A(u_m^-) \right] \right\}, \qquad [22]$$

$$(u_m^{\pm})^2 = \frac{1}{2R_m} \{ (r + (z \pm z_m)^2 - R_m^2)$$

$$+ [(r + (z \pm z_m)^2 - R_m^2)^2 + 4R_m^2 (z \pm z_m)^2]^{1/2} \},$$

and the fields are given by the expressions

$$E_1 = (V_1 - V_0)/z_1, \qquad E_3 = -E_2 = (V_2 - V_1)(z_2 - z_1), \qquad [23]$$

$$E_5 = -E_4 = (V_3 - V_2)/(z_3 - z_2).$$

The superposition (Eq. [22]) was obtained from linear combinations of Eq. [20] so that the uniform electric fields at $r \gg R$ are asymptotically correct. Certain restraints on the parameters are necessary to ensure accuracy of the approximation close to the axis (where electron trajectories cluster). For example, if only $V_5 \neq 0$ and $V_5 > 0$, then it can be shown that $z_4/R_4 < z_5/R_5$ is a necessary restraint, otherwise negative potentials will result on the axis. The problem is that a region close to $r = R_m$ and $z = z_m$ is incorrectly estimated and the extent of such a region can be obtained from a numerical analysis of Eq. [22].

A first test of the approximation has been to check if it predicts the proper cutoff voltage of $G2$ when $V_1 = -150V$, and V_3 is a fixed voltage of the order of 10 kV (different for different guns). The cutoff voltage is determined by the requirement that the E_z field at the center of the cathode be zero.

Six different gun BFRs have been tested, their parameters are listed in Table 2. The parameters t_1 and t_2 are the thickness of the $G1$ and $G2$ electrodes, whereas the spacings s_{01}, etc., pertain to those between the cathode and $G1$, etc. Certain details of BFR #4 not relevant to this study have been omitted. The cutoff voltages determined by the approximations in Eqs. [22] and [23] are given in Table 3.

The agreement between the analytical results based upon Eq. [22]

Table 2—Parameters of Test BFR's

	#1	#2	#3	#4	#5	#6
t_1	5.5	5	5	1	5	3
t_2	5.5	5	20	5	11	18.5
s_{01}	3	3	3	3	3	3
s_{12}	11.5	13	11.5	27	11	11.5
s_{23}	68	52	68	33	45	45
R_1	12.5	12.5	12.5	12.5	12.5	12.5
R_2	12.5	12.5	12.5	12.5	12.5	12.5
R_3	16	30	30	23	30	20
V_3(kV)	11.5	6.85	10.0	8.7	13.6	11.44

Table 3—Cutoff Voltages (Volts)

BFR	1	2	3	4	5	6
Numerical V_{co}	401	429	627	604	556	437
Analytical V_{co}	397	464	596	650	569	382

and the calculations by the computer program ELOP[8] range from good (#1, 3, 5) to fair (#2, 4, 6). However, fair agreement of V_{co} does not rule out good agreement of trajectory coordinates (see below).

We have also examined the effect of Laplace fields evaluated with Eq. [22] together with the transverse space-charge approximation (Eq. [11]) on numerical integration of the trajectory equations (Eq. [3]), in the BFR for the six different sets of BFR parameters tabulated in Table 2. The results for r are shown in Fig. 10, and those for $r' = dr/dz$ are compared with the full numerical analysis (the left column of each pair of columns) in Table 4. These trajectories originate from triplets of electrons emitted at the cathode at $r_c = m$ units from the center with $r_c' = 0$ (PR), $r_c' = 1$ (THU), and $r_c' = -1$ (THD). Their coordinates at the entrance plane ($z = 2$ units) of this calculation need not be specified here. Several conclusions can be drawn:

(1) It is evident from the last four columns of Table 4 (for BFR #6) that space charge is mainly responsible for the discrepancies between the numerical-field approximation in the left and the analytical-field approximation in the right of each pair of columns. Evidently, the approximation (Eq. [22]) by itself is good, even though the cutoff voltage of BFR #6 (see Table 3) is estimated somewhat low.

(2) Some of the discrepancies in r' may be due to the way Gaussians are fitted to the thermal distribution in Eq. [10]. Fig. 10 indicates a decrease in σ, and therefore larger errors in regions where the principal test electron does not lie between the two thermals, as one progresses from BFR #1 to BFR #6. The full numerical values of r are not shown; they agree quite well and the small discrepancies are not of importance compared with those in r' in determining the accuracy of trajectories deeper into the gun. Errors are largest

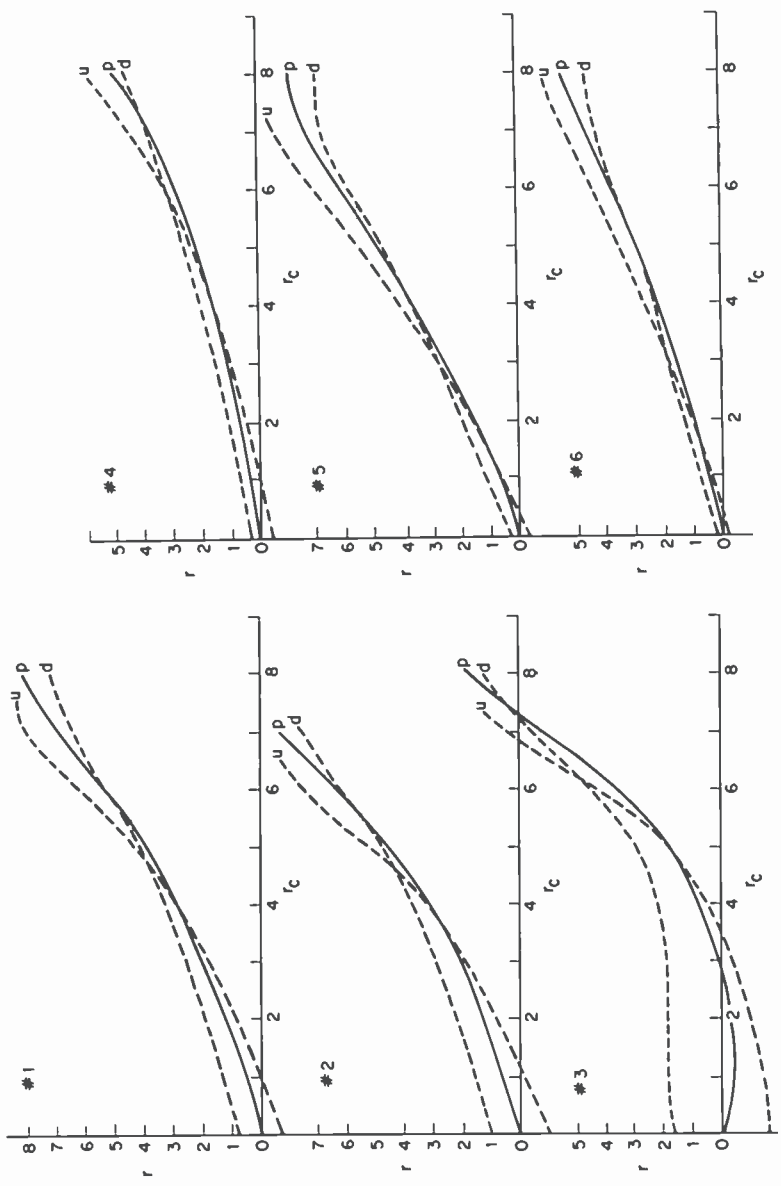

Fig. 10—Graphs of exit r versus cathode r_c for six BFR's. Each graph contains curves for one principal electron (p) and its two associated thermals (u,d).

Table 4—$r' \times 10^3$ for Six Test BFRs

		#1		#2		#3		#4		#5		#6		No Space Charge #6	
PR	1	−6.5	−3.7	−6.8	−2.1	1.1	3.7	−7.6	4.6	7.3	−5.1	−6.8	−5.8	−9.3	−8.7
PR	2	−13.9	−14.1	−14.4	−13.5	−1.9	−2.1	−15.6	−15.1	−15.2	−15.5	−14.7	−15.6	−18.3	−17.2
PR	3	−22.2	−24.1	−23.5	−23.7	−6.1	−9.1	−23.2	−24.7	−23.6	−25.7	−22.1	−25.3	−26.8	−25.4
PR	4	−31.3	−34.1	−33.9	−34.8	−12.1	−16.2	−31.2	−33.9	−32.1	−35.2	−29.8	−34.6	−34.3	−32.8
PR	5	−41.3	−44.3	−45.9	−45.6	−19.8	−23.0	−39.2	−43.5	−40.7	−44.4	−36.9	−42.9	−40.5	−39.0
PR	6	−52.0	−53.4	−58.8	−56.8	−30.2	−31.0	−47.3	−51.6	−49.1	−52.8	−43.1	−49.7	−44.2	−43.1
PR	7	−61.1	−62.3	−67.3	−66.6	−42.2	−40.0	−54.8	−59.0	−55.0	−59.8	−46.5	−53.2	−43.5	−43.3
PR	8	−6.00	−68.0			−43.6	−44.9	−58.2	−59.6	−48.9	−58.4	−39.0	−50.6	−32.8	−32.1
THU	0	3.5	1.9	3.9	5.5	8.1	7.8	−1.4	−1.2	−0.7	−1.6	−3.5	−5.2	−8.2	−10.9
THU	1	−5.3	−7.7	−5.3	−4.4	4.2	2.0	−10.0	−10.8	−10.0	−11.7	−11.9	−14.9	−17.5	−19.0
THU	2	−14.1	−17.5	−14.9	−15.4	−1.5	−4.1	−18.7	−20.6	−18.9	−21.8	−20.6	−24.7	−26.3	−27.5
THU	3	−23.9	−27.6	−26.1	−25.9	−7.5	−10.3	−27.2	−30.6	−28.4	−31.8	−29.4	−34.5	−34.7	−35.4
THU	4	−34.6	−37.8	−38.9	−37.2	−14.6	−17.3	−36.5	−40.3	−38.0	−41.9	−38.1	−44.2	−42.1	−42.4
THU	5	−46.4	−47.7	−53.4	−49.5	−23.2	−26.0	−45.9	−50.0	−47.3	−50.9	−45.5	−51.8	−47.3	−48.0
THU	6	−59.1	−64.7	−68.6	−62.4	−35.0	−33.7	−54.8	−58.4	−55.9	−59.9	−50.2	−58.4	−50.8	−51.2
THU	7	−68.6	−68.4			−48.2	−41.7	−61.5	−63.8	−60.6	−65.5	−50.9	−60.6	−48.2	−49.8
THD	0	−3.5	−1.9	−3.9	−5.5	−8.1	−7.8	1.4	1.2	0.7	1.6	3.5	5.2	8.2	10.1
THD	1	−10.9	−10.4	−12.8	−13.7	−11.8	−12.4	−6.8	−7.7	−7.3	−7.7	−4.6	−4.3	−1.0	−1.6
THD	2	−17.5	−18.7	−20.0	−21.7	−14.1	−15.4	−14.5	−16.9	−14.6	−15.8	−11.6	−13.5	−10.1	−7.0
THD	3	−24.4	−26.0	−27.2	−28.2	−15.5	−18.6	−21.9	−23.9	−21.9	−24.1	−18.4	−21.2	−18.5	−15.2
THD	4	−32.0	−33.8	−35.4	−35.1	−19.0	−20.5	−29.5	−31.8	−29.6	−32.2	−25.4	−40.4	−26.2	−22.9
THD	5	−40.2	−40.9	−44.4	−44.3	−24.8	−23.8	−36.7	−38.7	−37.2	−39.0	−31.9	−36.5	−32.5	−29.4
THD	6	−48.4	−50.2	−53.7	−54.2	−32.1	−30.9	−43.7	−45.8	−44.2	−47.6	−37.5	−41.1	−36.5	−34.1
THD	7	−54.9	−58.0	−58.1	−61.9	−39.7	−38.6	−49.7	−53.1	−48.4	−53.9	−39.9	−47.5	−36.3	−35.0
THD	8	−49.6	−62.2			−36.1	−42.4	−50.9	−51.4	−38.1	−50.4	−28.9	−43.1	−25.2	−23.5

for electrons emitted furthest from the cathode center, but concomitant current contributions from the edge electrons are small.

Thus, even though the effect of space charge is appreciable in the BFR and even though the transverse space-charge force approximation might not be accurate in the crossover region, it appears that fair to good predictions for electron coordinates at the end of the BFR can be made with these simplifying approximations.

The approximations ignore the effect of induced charges in the grids. Sample calculations show the effect of these to be negligible compared with other errors. The neglect of the longitudinal space-charge force was investigated in detail for BFR #6. Fig. 11 shows a comparison of both for the first 150 length units. Up to the crossover region (at $z \approx 50$ units), the neglect of longitudinal space-charge fields is somewhat serious, probably also accounting for some of the discrepancies. The rapid transition from longitudinally-dominant to transverse-dominant forces is quite apparent at the end of a diode region only a few length units long.

5. The Initial Equivalent-Diode Region

In this section, we present an approximate analysis of the difficult "diode region" of the BFR in which electron emission is space-charge

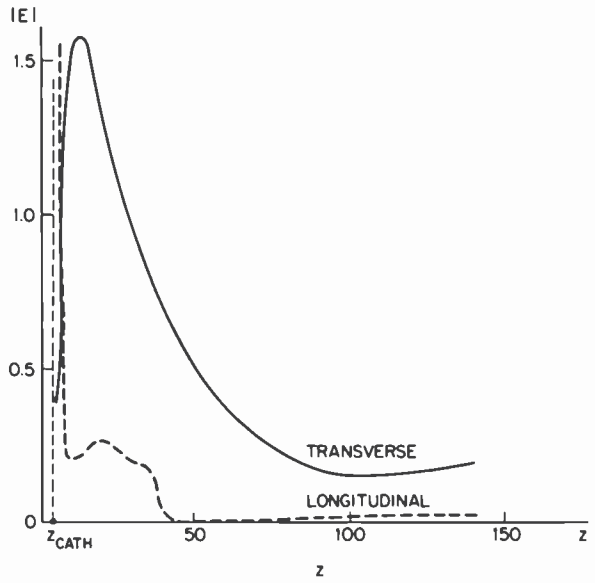

Fig. 11—A comparison in BFR #6 of longitudinal and transverse space-charge fields.

limited, i.e., the preceding cloud of emitted electrons shields its successor from the applied Laplace field so that the electric field at the cathode is essentially zero in the emitting region.

In the circularly symmetric cathode vicinity, the Laplace potential can be written as

$$\begin{aligned}\Phi^{L}(r, z) &= \Phi^{L}(0, z) - \tfrac{1}{4}r^2\Phi''(0, z) \\ &= \Phi^{L}(0, z)[1 - r^2/R_c^2],\end{aligned} \tag{24}$$

to the extent that r^4 and higher-order terms may be neglected. This equality gives a working definition of an effective cathode radius R_c. For $r \ll R_c$, Eq. [24] is a two-term expansion of

$$\Phi^{L}(r, z) = J_0(2r/R_c)\Phi^{L}(0, z). \tag{25}$$

One can verify that Eq. [25]) is the solution of the Laplace equation if $\Phi^{L}(0, z)$ is a linear combination of $\sinh(2z/R_c)$ and $\cosh(2z/R_c)$. Hence, an acceptable solution of $\Phi(r, z)$ with $\Phi^{L}(0, z) = V_c$ is

$$\Phi^{L}(r, z) = V_c + v \sinh(2z/R_c) J_0(2r/R_c), \tag{26}$$

where v is an unknown constant voltage determined by the geometry. Fields[23] made the crucial point that the situation in the BFR very close to the cathode is indistinguishable from one in an effective diode where an anode at voltage V_A at some distance d_A produces Eq. [26] as well as the proper solution to the Poisson equation close to the cathode. That is to say, Eq. [26] can be rewritten in terms of this equivalent diode as,

$$\Phi^{L}(r, z) = V_c + (V_A - V_c)\frac{\sinh(2z/R_c)}{\sinh(2d_A/R_c)} J_0(2r/R_c), \tag{27}$$

even though this predicts the Laplace potential correctly only for an immediate vicinity of the cathode center. In the case of a purely one-dimensional situation ($R_c \to \infty$) it can be seen[23] from Eq. [27] that d_A reduces to the length $d_0 = [\partial E_z^{L}(0, 0)/dV_c]^{-1}$. On the other hand, Eq. [27] yields

$$\frac{\partial E_z^{L}(0, 0)}{\partial V_c} = \frac{2/R_c}{\sinh(2d_A/R_c)}, \tag{28}$$

so that by inversion we relate an effective diode length d_A to the physical length $d_0 \equiv [\partial E_z^{I}(0, 0)/dV_c]^{-1}$,

$$\begin{aligned}d_A &= \tfrac{1}{2}R_c \ln[(2d_0/R_c) + (1 + 4\, d_0^2/R_c^2)^{1/2}] \\ &= \tfrac{1}{2}R_c \operatorname{arc}\sinh(2d_0/R_c).\end{aligned} \tag{29}$$

Note that d_0 is entirely determined by the geometry and the Laplace fields of the real problem, where d_A also contains the curvature radius R_c which will later be replaced by an effective beam radius.

Close to the cathode, the fields are governed by the Poisson equation,

$$\frac{\partial^2\Phi}{\partial z^2} + \frac{1}{r}\frac{\partial}{\partial r}\left(r\frac{\partial\Phi}{\partial r}\right) = \frac{1}{\epsilon_0}\rho(r, z) \approx 2\pi\beta\frac{j(r, z)}{\Phi^{1/2}}, \qquad [30]$$

where $j(r, z)$ is the current density and β is the constant given in Eq. [9]. If $\Phi(r, z)$ has $J_0(2r/R_c)$ as a factor containing all the dependence upon r, then the correct solution of Eq. [30] can be written

$$j(r) = \frac{2}{9\pi\beta}\frac{[\Phi(r, z) - V_c]^{3/2}}{\bar{R}_c^2[\sinh(z/\bar{R}_c)]^2}, \qquad [31]$$

where $\bar{R}_c = 2R_c/3$. Now we apply Eq. [31] at $z = d_A$, the effective anode position, and replace the numerator, using Eq. [27],

$$\Phi(r, d_A) - V_c = \tfrac{1}{2}R_c[-E_z^L(r, 0)]\sinh(2d_A/R_c) \qquad [32]$$

to obtain the following analytical expression for the estimated current density:

$$j(r) = \frac{2}{9\pi\beta}[-E_z(r, 0)]^{3/2}D^{-1/2},$$
$$D = \frac{128}{81}R_c\frac{[\sinh(3d_A/2R_c)]^4}{[\sinh(2d_A/R_c)]^3}, \qquad [33]$$

where d_A is given by Eq. [29] and $d_0 \equiv (\partial E_z^L/\partial V_c)^{-1}$ at the center of the cathode. The remarkable aspect of Eq. [33] is that the estimate does not require a lengthy iterative numerical simulation by computer; only the Laplace fields $E_z(r, 0)$ are needed and they are easily obtained from the approximations in the previous section. However, several defects in the assumptions must be borne in mind:

(1) The assumption that potential and current are proportional to $J_0(2r/R_c)$ is incorrect for values of r close to R_c. Fortunately $j(r)$ is very small when $|R_c - r| \ll R_c$.

(2) The curvature radius R_c is close to, but not equal to the effective beam radius, and furthermore R_c is a decreasing function of z in the diode region (in contrast to the constant R_c assumed in developing Eq. [32]). Table 5 shows predictions of $j_c(r)$ made on the basis of Eq. [33] with an ad hoc adjustment for the above points by replacement of R_c in Eq. [33] by $\tilde{R}_c$ [~70% of the actual beam radius obtained from the location on the cathode where $E_z^L(r, 0) = 0$)]. Each pair of columns gives the numerically approximated current (density) to the left and the analytically estimated one to the right. The current density $J_c(m) = 2\pi\beta j_c(mh)$,

where $h = 1$ unit, and $2\pi\beta \approx 190.43$ if $j_c(mh)$ is to be in mA. The total current I in mA is also given.

When reasonably accurate densities have been established by this procedure, we then use Eq. [3] to simulate electron trajectories in the short diode region, with a version of Eq. [31] that gives the Child's law potential and fields in terms of the estimated current densities. At the end of the diode region, a transition is made to the transverse space-charge approximation. This abruptness of the transition, exemplified in Fig. 11, makes it possible to estimate its location from experience with an entire class of not-dissimilar cathode-$G1$ regions.

Table 5—Current Densities Predicted by Eq. [33] Compared with Computer-Determined Ones

	#1		#2		#3		#4		#5		#6	
I(mA)	3.50		2.02		3.48		3.55		3.73		3.47	
$J_c(0)$	6.41	6.06	4.37	4.40	6.21	6.45	5.09	6.72	6.66	6.98	5.66	5.95
$J_c(1)$	6.31	5.97	4.30	4.32	6.12	6.34	5.05	5.65	6.57	6.86	5.60	5.87
$J_c(2)$	6.02	5.69	4.06	4.06	5.85	6.03	4.91	5.44	6.28	6.51	5.40	5.62
$J_c(3)$	5.53	5.24	3.68	3.64	5.41	5.50	4.69	5.07	5.79	5.93	5.07	5.20
$J_c(4)$	4.85	4.60	3.14	3.07	4.77	4.77	4.35	4.56	5.11	5.13	4.58	4.61
$J_c(5)$	3.96	3.80	2.44	2.35	3.93	3.85	3.87	3.86	4.21	4.13	3.91	3.83
$J_c(6)$	2.89	2.86	1.62	1.54	2.90	2.77	3.22	2.97	3.11	2.96	3.03	2.87
$J_c(7)$	1.69	1.81	0.69	0.69	1.72	1.60	2.37	1.91	1.87	1.70	1.96	1.77
$J_c(8)$	0.47	0.76			0.48	0.49	1.29	0.76	0.56	0.53	0.72	0.65

6. Conclusions

The purpose of this work has been to replace accurate but costly numerical simulation (by digital computer) of electron trajectories in kinescope guns by analytical approximations to provide the gun designer with a flexible, low-cost, exploratory tool. We have found that space-charge forces can be approximated by transverse electric fields in typical kinescope beams at high accuracy beyond the crossover region in the BFR. Between the cathode and the crossover region, the transverse-field approximation is somewhat (but not seriously) in error, as long as the immediate vicinity is properly treated separately as an effective diode. For this reason, it is emphasized that the approximations in this work are most useful in the drift region, and in the main-lens region when circularly symmetric cylinder lenses of equal radius are utilized.

Cathode current distributions can be estimated from the Laplace fields. These, in turn, can be approximated analytically in axially symmetric guns with conventionally shaped grids and lenses. While such analytical approximations also carry with them some loss in accuracy, they provide a tremendous gain in time and cost, and therefore are especially useful for exploratory design in which high

accuracy (well within 10% of the ELOP numerical calculations) is not yet necessary.

Acknowledgements

I am grateful to R. W. Cohen whose interest in a simplified analysis spurred me on to attempt the present one, to C. H. Anderson for inducing me to refine the space-charge approximation, and to R. C. Alig and F. J. Campbell for critical discussions and review of this work.

References

[1] C. Weber, "Numerical Solution of Laplace's and Poisson's Equations and the Calculation of Electron Trajectories and Electron Beams," in *Focussing of Charged Particles*, A. Septier (Ed.), Academic Press, N.Y. (1967).
[2] P. W. Hawkes, "Compilation of a Catalogue of Computer Programs in Electron Optics," *Computer Phys. Commun.*, **5**, p. 399 (1973).
[3] Any of the classical treatises on electron optics, e.g., V. K. Zworykin, G. A. Morton, E. G. Ramberg, J. Hillier, A. W. Vance, *Electron Optics and the Electron Microscope*, J. Wiley, N.Y. (1945).
[4] D. Potter, *Computational Physics*, J. Wiley, N.Y. (1977); R. W. Hockney, J. W. Eastwood, *Computer Simulation Using Particles*, McGraw-Hill, N.Y. (1981).
[5] M. A. Jaswon and G. T. Symm, *Integral Equation Methods in Potential Theory and Elastostatics*, Academic Press, London, U.K. (1977).
[6] P. Grivet, *Electron Optics* (2nd English Ed.), Pergamon Press, Oxford, U.K. (1972).
[7] T. Saito S. Kubota, and S. Miyaoka, "Digital Computer Studies of Electron Lenses for Cathode Ray Tubes," *J. Appl. Phys.*, **44**, p. 4504 (1973).
[8] F. J. Campbell, private communication; see also R. H. Hughes and H. Y. Chen, "A Novel High-Voltage Bipotential CRT Gun Design," *IEEE Trans. Consumer Electron.*, **CE-25**, p. 185 (1979).
[9] D. L. Say, R. B. Jaeger, and J. D. Ryan, "Electron Optics for CRT's: Computer Modeling," *IEEE Trans. Consumer Electron.*, **CE-21**, p. 57 (1975).
[10] R. C. Alig, "Kinescope Electron Gun Design," *RCA Review*, **41**, p. 517 (1980).
[11] S. Bertram, "Determination of the Axial Potential Distribution in Axially Symmetric Electrostatic Fields," *Proc. IRE*, **28**, p. 418 (1940). See also Ref. (6), Sec. 8.1.
[12] E. Regenstreif, "Theorie de la Lentille Électrostatique à Trois Électrodes," *Ann. Radioel.*, **6**, p. 51 (1951).
[13] J. D. Lawson, *The Physics of Charged-Particle Beams*, Clarendon, N.Y. (1977).
[14] E. G. Ramberg in Ref. (3), Sec. 12.1.
[15] K. J. Harte, "Theory of Aberration Mixing in Electron-Optical Systems," *J. Vac. Sci. Technol.*, **10**, p. 1098 (1973).
[16] A. B. El-Kareh and J. C. J. El-Kareh, *Electron Beams, Lenses, and Optics*, Academic Press, N.Y. (1970) (see Sec. 3.5).
[17] R. W. Klopfenstein, private communication.
[18] Ref. (6), formula (8.1).
[19] W. Franzen, J. H. Porter, "Energy Spectrum of Electrons Emitted by a Hot Cathode," in L. Morton (Ed.) *Advances in Electronics and Electron Physics*, Vol. 39, Academic Press, N.Y. (1975).
[20] O. Klemperer, *Electron Optics*, Cambridge, U.K. (1971).
[21] E. G. Ramberg in Ref. (3), Sec. 11.8.
[22] Ref. (6), Sec. 8.2.
[23] J. R. Fields, private communication. Fields first pointed out the connection between $(\partial E_z^L/\partial V_c)^{-1}$ and an effective diode width.